

Small Bites: Star formation recipes in extreme dwarfs

Sambit Roychowdhury,^{1*} Jayaram N. Chengalur,^{1*} Serafim S. Kaisin,^{3*} Ayesha Begum,^{2*} and Igor D. Karachentsev^{3*}

¹NCRA-TIFR, Post Bag 3, Ganeshkhind, Pune 411 007, India

²Dept of Astronomy, University of Wisconsin-Madison, Madison WI 53706-1582

³Special Astrophysical Observatory, Russian Academy of Sciences, N. Arkhyz, KChR 369167, Russia

ABSTRACT

We study the relationship between the gas column density (Σ_{HI}) and the star formation rate surface density (Σ_{SFR}) for a sample of extremely small ($M_{\text{B}} \sim -13$, $\Delta V_{50} \sim 30 \text{ km s}^{-1}$) dwarf irregular galaxies. We find a clear stochasticity in the relation between the gas column density and star formation. All gas with $\Sigma_{\text{HI}} \gtrsim 10 M_{\odot} \text{ pc}^{-2}$ has some ongoing star formation, but the fraction of gas with ongoing star formation decreases as the gas column density decreases, and falls to about 50% at $\Sigma_{\text{HI}} \sim 3 M_{\odot} \text{ pc}^{-2}$. Further, even for the most dense gas, the star formation efficiency is at least a factor of ~ 2 smaller than typical of star forming regions in spirals. We also find that the ratio of $\text{H}\alpha$ emission to FUV emission increases with increasing gas column density. This is unlikely to be due to increasing dust extinction because the required dust to gas ratios are too high. We suggest instead that this correlation arises because massive (i.e. $\text{H}\alpha$ producing) stars are formed preferentially in regions with high gas density.

Key words: galaxies: dwarf – galaxies: irregular – radio lines: galaxies

1 INTRODUCTION

Models of galaxy formation and evolution generally use semi-empirical “recipes” to follow the process of star formation (e.g. Springel et al. 2005; Governato et al. 2010). Typically, star formation is assumed to set in only above a “threshold” gas (column) density Σ_{gas} and beyond that to be proportional to a power of Σ_{gas} . This is supported by observations of nearby star forming galaxies (e.g. Schmidt 1959; Kennicutt 1998). However, most of these observations are of large spiral galaxies, whereas from the hierarchical galaxy formation model one would expect that the first formed systems were much smaller than the typical $z \sim 0$ spiral. Here we study the relation between gas and star formation in nearby, extremely faint ($M_{\text{B}} \sim -13$, $\Delta V_{50} \sim 30 \text{ km s}^{-1}$) gas rich dwarfs.

The dwarf galaxies in our sample are dynamically and structurally very different from the large spiral galaxies for which the widely used star formation recipes have been derived. Firstly, in our sample galaxies the rotation velocity is not much larger than the velocity dispersion (e.g. Begum, Chengalur, & Hopp 2003; Begum et al. 2008). Further, the gas does not settle into a thin disc; the mean observed axial ratio of the gas discs is ~ 0.6 (Roychowdhury et al. 2010). Both this as well as the expectation that negative feedback from supernovae would play a more important role in small galaxies (e.g. Mac Low & Ferrara 1999) make it

likely that the relationship between the gas density and star formation in dwarf galaxies is different from that in spirals.

Observationally, there is another major difference between studies of star formation recipes in dwarf galaxies and spirals. Molecular gas is almost never detected in dwarf galaxies (e.g. Taylor, Kobulnicky, & Skillman 1998), which means that the gas column density has to be estimated from the HI column density Σ_{HI} alone. On the other hand, in large spirals, the star formation appears to be governed by the molecular gas density and to be much less (if at all) related to the atomic gas (e.g. Wong & Blitz 2002; Leroy et al. 2008). However, in Roychowdhury et al. (2009) (henceforth R09) we showed that for dwarf galaxies, in regions of active star formation, the star formation rate Σ_{SFR} is correlated to the HI column density, albeit with significant scatter. R09 also found that there was no sharp “threshold” for star formation, with star formation proceeding at all gas column densities, down to the sensitivity limit of the data. Similarly, Bigiel et al. (2010) find that in the HI dominated outskirts of spiral galaxies, the SFR and HI are correlated, albeit with a scatter.

In this paper we extend our previous work in two important directions. Firstly we try to quantify the stochastic nature of the relationship between Σ_{SFR} and Σ_{HI} . Secondly we also study the relationship between the gas column density and the formation of stars of different masses.

* E-mail: sambit@ncra.tifr.res.in (SR); chengalu@ncra.tifr.res.in (JNC); skai@sao.ru (SSK); begum@astro.wisc.edu (AB); ikar@sao.ru (IDK)

Table 1. The sample

Galaxy	M_B (mag)	Dist (Mpc)	Group	a ($'$)	b/a
UGC 685	-14.31	4.5	Field	1.4	0.71
KK 14	-12.13	7.2	N672	1.6 ⁺	0.37
UGC 3755	-14.90	6.96	Field	1.7	0.59
KK 65	-14.29	7.62	Field	0.9 ⁺	0.56
UGC 4459	-13.37	3.56	M81	1.6	0.87
UGC 6456	-14.03	4.3	M81	1.5	0.53
KK 144	-12.59	6.3	CVn I	1.5 ⁺	0.33
DDO 125	-14.16	2.5	CVn I	4.3	0.56
UGC 7605	-13.53	4.43	CVn I	1.1	0.73
DDO 181	-13.03	3.1	CVn I	2.3	0.57
KKH 98	-10.78	2.5	Field	1.1 ⁺	0.55

⁺: diameters correspond to the Holmberg system ($26.5 \text{ mag arcsec}^{-2}$)

2 SAMPLE AND DATA ANALYSIS

Our sample consists of 23 galaxies drawn from the GMRT¹ FIGGS HI 21cm survey (Begum et al. 2008) with UV data from *GALEX*.² See R09 for details. For 11 of these 23 galaxies $H\alpha$ data from the 6m BTA telescope in Russia is available. The full sample has median HI mass $M_{HI} \sim 28 \times 10^6 M_\odot$, median blue magnitude $M_B \sim -13.2$, and median velocity width $\Delta V_{50} \sim 32 \text{ km s}^{-1}$. The corresponding values for the $H\alpha$ subsample is $M_{HI} \sim 34 \times 10^6 M_\odot$, $M_B \sim -13.5$, $\Delta V_{50} \sim 33 \text{ km s}^{-1}$. The galaxies with $H\alpha$ observations are listed in Table 1; the columns in the table are: Column(1) the galaxy name, Column (2) the absolute blue magnitude (corrected for galactic extinction, the internal extinction correction has been assumed to be negligible), Column(3) the distance in Mpc, Column(4) the group membership of the galaxy. All of this data has been taken from Begum et al. (2008). Column(5) the de Vaucouleurs (25 mag/arcsec^2) diameter of the optical disc. For dwarf low surface brightness galaxies from the KK lists (KK14, KK65, KK144, KKH98), the diameters correspond to the Holmberg system ($26.5 \text{ mag arcsec}^{-2}$). Column(6) the optical axis ratio. Data for columns (5) and (6) have been taken from taken from Karachentsev et al. (2004).

Background corrected *GALEX* FUV band (1350-1750 Å) images were converted into luminosity units using the calibration information provided at the *GALEX* site. Correction for galactic extinction was done using extinction values of Schlegel, Finkbeiner & Davis (1998) and using formulae from Cardelli, Clayton & Mathis (1989) to extrapolate to the FUV band. No correction for internal extinction was made, since our sample galaxies are expected to be extremely dust poor. The luminosity values thus obtained were converted to star formation rates using the calibration given in Kennicutt (1998a) :

$$\text{SFR}(M_\odot \text{ year}^{-1}) = 1.4 \times 10^{-28} L_\nu \text{ (ergs s}^{-1} \text{ Hz}^{-1}) \quad (1)$$

¹ We thank the GMRT staff for having made possible the observations used in this paper. The GMRT is run by the National Centre for Radio Astrophysics of the Tata Institute of Fundamental Research.

² Some of the data presented in this report were obtained from the Multi-mission Archive at the Space Telescope Science Institute (MAST). STScI is operated by the Association of Universities for Research in Astronomy, Inc., under NASA contract NAS5-26555. Support for MAST for non-HST data is provided by the NASA Office of Space Science via grant NAG5-7584 and by other grants and contracts.

In deriving this calibration it is assumed that the stellar distribution has solar metallicity and a Salpeter IMF, and that the galaxy has had continuous star formation over time scales of 10^8 years or longer. The implications of these assumptions are discussed in Section 3.

Details of the $H\alpha$ data reduction can be obtained from Karachentsev & Kaisin (2007) and Kaisin & Karachentsev (2008). The images were corrected for dust extinction due to our own Galaxy in a similar way as was done for the FUV maps. The $H\alpha$ luminosity was converted to star formation rates using the calibration given in Kennicutt (1998a) :

$$\text{SFR}(M_\odot \text{ year}^{-1}) = 7.9 \times 10^{-42} L_{H\alpha} \text{ (ergs s}^{-1}) \quad (2)$$

The assumptions used to derive this calibration are the same as that used in deriving the FUV flux -SFR calibration

For data from all the three wavelengths, relevant parameters (Σ_{HI} and Σ_{SFR}) were calculated over several scales, viz. a) an average over the entire star forming disc of the respective galaxy (i.e. “global” values). The “star forming disc” is defined as that within the radius at which the star formation rate is $1.85 \times 10^{-4} M_\odot \text{ yr}^{-1} \text{ kpc}^{-2}$ (as measured from the FUV flux, with the *GALEX* images smoothed to 400 pc linear resolutions). This approximately corresponds to the B band Holmberg diameter for those sample galaxies for which the Holmberg diameter has been measured. b) “pixel” values. We use “pixels” that Nyquist sample squares 400 pc or 150 pc in size. For the HI images 400 pc resolution images are available for all the galaxies in our sample. Similarly for the FUV data, 150 pc resolution images are available for all galaxies.

Figure 1 shows $H\alpha$ greyscale images overlaid with FUV and HI contours, for a representative galaxy in our sample.

3 RESULTS AND DISCUSSION

Figure 2[A] shows the relationship between the disc-averaged $\Sigma_{SFR}^{H\alpha}$ (and corresponding Σ_{SFR}^{FUV}) and Σ_{HI} for the galaxies in our sample with $H\alpha$ data. Note that the galaxies are forming stars even though their typical gas density is at or below the “threshold density”. Panel [B] shows how the global Σ_{SFR} estimates obtained using the two different tracers relate. Although the SFR tracers do correlate, there is a considerable scatter about the 1:1 line. Note that the data agrees better with the original calibration suggested by Kennicutt (1998a) than with the re-calibration suggested by Lee et al. (2009), though it should be noted that the latter sample is much larger than ours. In terms of total SFR the values range from $2.79 \times 10^{-4} M_\odot \text{ yr}^{-1}$ to $1.05 \times 10^{-2} M_\odot \text{ yr}^{-1}$ with FUV as tracer, and from $2.33 \times 10^{-4} M_\odot \text{ yr}^{-1}$ to $1.21 \times 10^{-2} M_\odot \text{ yr}^{-1}$ with $H\alpha$ as tracer. Finally, following Hunter, Elmegreen & Ludka (2010) we show in Panel [C] the ratio $\Sigma_{SFR}^{FUV}/\Sigma_{SFR}^{H\alpha}$ as a function of $\Sigma_{SFR}^{H\alpha}$. There is a clear correlation and the best fit line has a slope of -0.63 ± 0.09 , (compared to -0.59 obtained by Hunter, Elmegreen & Ludka (2010)). The SFR calibration we used assumes solar metallicity, however, as discussed in detail by Hunter, Elmegreen & Ludka (2010), the fact that the dwarf galaxies have lower than solar metallicity has only a marginal effect on the $\Sigma_{SFR}^{FUV}/\Sigma_{SFR}^{H\alpha}$ ratio, since both calibrations are similarly affected.

In what follows we take a look at the relationship between gas and star formation on small scales, by making “pixel-by-pixel” comparisons of Σ_{HI} and Σ_{SFR} . We first focus on stochasticity in the star formation and return to the comparison between $\Sigma_{SFR}^{H\alpha}$ and Σ_{SFR}^{FUV} in Sec. 3.2.

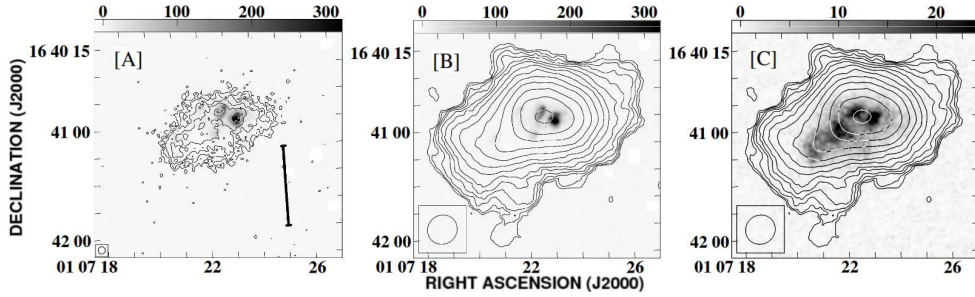


Figure 1. Overlays of the H α , UV and HI images for UGC685. [A]Greyscales H α (in 10^{-18} ergs s $^{-1}$ per pixel of area 0.1225 arcsecond squared), contours GALEX FUV image (from 0.0014 to 0.032 cps per pixel of area 2.25 arcsecond squared, in steps of 2). [B]Greyscales H α , contours GMRT HI image (from 17.5 to 1120 Jy/bm \times m/s in steps of $\sqrt{2}$). [C]Greyscales GALEX FUV (in 10^{-3} cps per pixel of area 2.25 arcsecond squared), contours GMRT HI image. Respective resolutions are, H α : 1.9'', FUV: 4'', HI: 17'' \times 16''. The length of the bold line in panel [A] is approximately 1 Kpc.

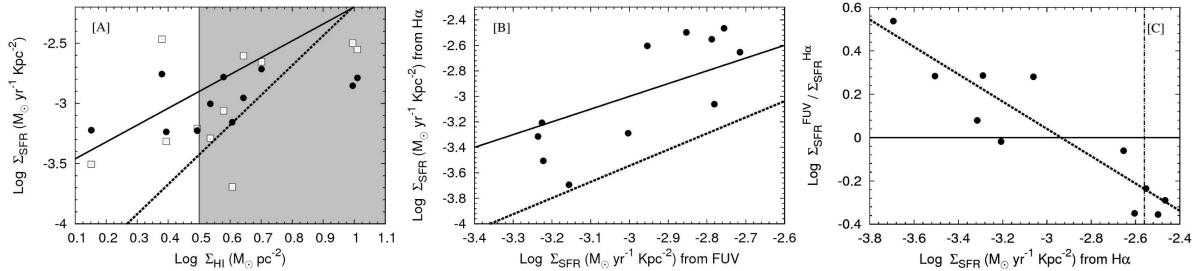


Figure 2. [A] Σ_{SFR} derived from H α ($\Sigma_{\text{SFR}}^{\text{H}\alpha}$, empty squares) and FUV ($\Sigma_{\text{SFR}}^{\text{FUV}}$, filled circles) plotted against Σ_{HI} , assumed to represent Σ_{gas} , both axes being in log scale. The solid line represents the Kennicutt-Schmidt law with a slope of 1.4, and the dashed line represents the best fit Schmidt law for spiral galaxies only, both taken from Kennicutt (1998). The shaded region covers various estimates of the “threshold density” tabulated in Kennicutt (1989). [B]Disc-averaged values of $\Sigma_{\text{SFR}}^{\text{H}\alpha}$ and $\Sigma_{\text{SFR}}^{\text{FUV}}$. The solid line is the 1:1 line, and the dashed line represents the relationship found by Lee et al. (2009). [C]Ratio of global $\Sigma_{\text{SFR}}^{\text{FUV}}/\Sigma_{\text{SFR}}^{\text{H}\alpha}$ as a function of $\Sigma_{\text{SFR}}^{\text{H}\alpha}$. The dashed line is the best fit straight line and has a slope of -0.63. The vertical dot-dashed line shows the approximate Σ_{SFR} value for our sample galaxies for which the SFR estimated assuming a Salpeter IMF will start deviating from the true SFR according to Pflamm-Altenburg, Weidner & Kroupa (2007). See the text for more details.

3.1 Stochasticity in Star Formation

R09 showed that from a comparison of the FUV and HI images, in star forming regions $\Sigma_{\text{SFR}}^{\text{FUV}}$ and Σ_{HI} are related as

$$\log \Sigma_{\text{SFR}}^{\text{FUV}} = (1.81 \pm 0.05) \log \Sigma_{\text{HI}} - 4.70 \pm 0.05 \quad (3)$$

By comparison with the canonical K-S law

$$\log \Sigma_{\text{SFR}} = (1.4 \pm 0.15) \log \Sigma_{\text{gas}} - 3.60 \pm 0.14 \quad (4)$$

and noting that (i) Σ_{HI} is a strict lower limit to the total Σ_{gas} and (ii) for a given FUV flux the inferred SFR decreases with decreasing metallicity, the robust conclusion that one can draw is that the star formation process in dwarf galaxies is significantly less efficient than that in big galaxies. R09 also showed (see their Fig. 6) that the data implied stochasticity and were best modelled as a stochastic power law with a variation of 50% in the coefficient (as opposed to the slope) of the power law. Begum et al. (2006) had also highlighted the stochasticity in the relation between Σ_{SFR} and Σ_{HI} in dwarf galaxies. To properly characterize the star formation process, one would hence also need to know the average fraction of the gas that is participating in the star formation process.

Figure 3 shows the fraction of pixels which are observed to be star forming (i.e. have a star formation rate of at least 3σ , where σ is the rms in the UV image, in units of the star formation rate). The plot averages over 16 of the original sample of 23 galaxies, 7

galaxies with relatively low GALEX exposure times have been excluded. The dashed vertical lines indicate the rms level (after being translated from Σ_{SFR} to Σ_{HI} using Eqn. 3). For a given galaxy, if there was no stochasticity in the star formation, all points above the rms level (right of the corresponding dashed line) should have had observable star formation. As such, all points to the right of the rightmost dashed line can hence be regarded as giving a reliable fraction of gas that is participating in star formation. There are several points worth noting, viz. (1) all pixels with gas density greater than $\sim 10 \text{ M}_{\odot}/\text{pc}^2$ participate in star formation. Interestingly, this number is identical to the threshold density for star formation of $\sim 10^{21}$ atoms/cm 2 proposed by Skillman (1987), (2) the fraction of gas which participates in star formation decreases nearly linearly with decreasing Σ_{HI} ($f_{\text{SF}} = 0.96 \log \Sigma_{\text{HI}} + 0.1$). (3) even for a gas density $\log \Sigma_{\text{HI}} \sim -1.0$, two orders of magnitude below the usually assumed threshold for star formation, at least 5% of the gas is observed to be forming stars. The average Σ_{HI} for the pixels with $\Sigma_{\text{HI}} > 10 \text{ M}_{\odot}/\text{pc}^2$ is $\sim 17.3 \text{ M}_{\odot}/\text{pc}^2$, and the average Σ_{SFR} for these pixels is $3.5 \times 10^{-3} \text{ M}_{\odot}/\text{yr}/\text{kpc}^2$. Thus even for the densest gas in dwarf galaxies, the star formation efficiency (i.e. $\Sigma_{\text{SFR}}/\Sigma_{\text{gas}}$) is hence $\sim 2.0 \cdot 10^{-10} \text{ yr}^{-1}$, about a factor of two lower than the typical value for spiral galaxies (Leroy et al. 2008).

3.2 Massive star formation

FUV emission is sensitive to the SFR of intermediate mass ($M \gtrsim 3 \text{ M}_{\odot}$) relatively long lived (lifetime $\sim 10^8 \text{ yr}$) stars. H α emission on the other hand traces the instantaneous SFR of massive

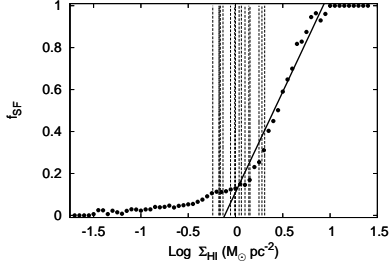


Figure 3. Plot of the fraction of gas that is “participating in star formation” as a function of Σ_{HI} . The plot averages over 16 galaxies, the dashed horizontal lines indicate the rms level of the UV images of the individual galaxies (after being translated from Σ_{SFR} to Σ_{HI} using Eqn. 3). All points to the right of the rightmost dashed line can be regarded as giving a reliable fraction of gas that is participating in star formation. The solid line is a fit to the “reliable” points. See text for more details.

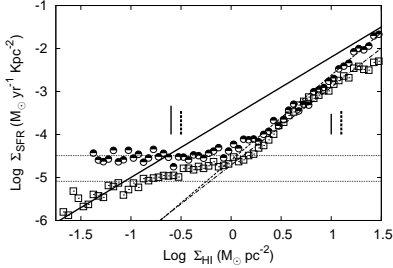


Figure 4. Plots showing the binned 400pc resolution $\Sigma_{\text{SFR}}^{\text{FUV}}$ (hollow squares) and $\Sigma_{\text{SFR}}^{\text{H}\alpha}$ (half-filled circles) as a function of Σ_{HI} . The $\Sigma_{\text{SFR}}^{\text{FUV}}$ data are for the 23 galaxies listed in R09, where as the $\Sigma_{\text{SFR}}^{\text{H}\alpha}$ data are for the 11 galaxies listed in Table 1. The average sensitivity levels for the two sets of data are indicated by the respective horizontal lines. The dashed and the dot-dashed lines show the Schmidt law fit to the $\text{H}\alpha$ and FUV data respectively. The solid line is the canonical K-S law (Eqn. 4). The typical 1σ scatter either above or below the mean in each bin is indicated by the vertical lines, in (1) the power law and (2) sensitivity limited parts for both tracers. Dashed lines are for $\text{H}\alpha$ data, bold lines are for FUV data. Note that points with negative or zero FUV flux have been dropped from the plots.

($M \gtrsim 17M_{\odot}$) short lived (lifetime $\sim 10^6$ yr) stars. For our sample galaxies we show in Fig. 4 the Σ_{SFR} as deduced from the FUV emission ($\Sigma_{\text{SFR}}^{\text{FUV}}$), as well as $\text{H}\alpha$ emission ($\Sigma_{\text{SFR}}^{\text{H}\alpha}$) as a function of Σ_{HI} at a resolution of 400pc. (Note that pixels corresponding to gas not taking part in star formation, i.e. with negative or zero FUV flux, are not included in this plot) The best fit power laws to the $\text{H}\alpha$ data is given by:

$$\log \Sigma_{\text{SFR}}^{\text{H}\alpha} = (1.98 \pm 0.04) \log \Sigma_{\text{HI}} - 4.60 \pm 0.05 \quad (5)$$

As can be seen the $\Sigma_{\text{SFR}}^{\text{H}\alpha}$ and $\Sigma_{\text{SFR}}^{\text{FUV}}$ points overlap within the scatter (indicated by the vertical line). Nonetheless as a comparison of Eqn. 5 and Eqn. 3 shows, there is a significant difference ($\sim 2.7\sigma$, where σ is the quadrature sum of the individual errors) in the slope of the two relationships, with the $\Sigma_{\text{SFR}}^{\text{H}\alpha}$ relation being steeper.

Discrepancies between the SFR rates deduced between these two tracers have been investigated earlier by several authors, including, for e.g. Meurer et al. (2009); Pflamm-Altenburg, Weidner & Kroupa (2009); Lee et al. (2009). A number of explanations for the two rates to diverge have been

suggested, including (i) Stochastic paucity of high mass stars at low star formation rates. This would make $\Sigma_{\text{SFR}}^{\text{H}\alpha}$ at low star formation rates lower than $\Sigma_{\text{SFR}}^{\text{FUV}}$. For example Lee et al. (2009) show that for star formation rates lower than $\sim 10^{-2}M_{\odot}/\text{yr}$, the $\text{H}\alpha$ emission systematically under predicts the true SFR. (ii) Non uniform star formation rates. For example if the star formation is bursty, then a few million years after the burst all the OB stars would have died and the $\text{H}\alpha$ emission would once again systematically underestimate the true SFR. (iii) leakage of ionizing photons, either out of the galaxy, or into a more diffuse region of the ISM, where the resulting $\text{H}\alpha$ emission has too low a surface brightness to be detected (e.g. Melena et al. (2009)). Once again, this would result in the $\text{H}\alpha$ emission underestimating the true SFR. (iv) variations in the IMF. For example, Meurer et al. (2009) identify correlations between $\Sigma_{\text{SFR}}^{\text{FUV}}/\Sigma_{\text{SFR}}^{\text{H}\alpha}$ with global galaxy parameters like the luminosity, rotational velocity and dynamical mass, and argue that this implies an IMF that varies with environment. Weidner & Kroupa (2005) present a model in which the underlying IMF is universal, but a dependence of the most massive star formed in a cluster on the mass of the cluster leads to the total stellar population having a steeper IMF than the canonical one. (v) Dust extinction. Since dust extinction is more at the shorter wavelengths, under correction for dust would lead to the FUV emission underestimating the true SFR. Note that in most of the above scenarios the $\text{H}\alpha$ emission would under predict the true star formation rate. One would expect the $\Sigma_{\text{SFR}}^{\text{H}\alpha}$ to exceed $\Sigma_{\text{SFR}}^{\text{FUV}}$ (as observed for about half of our sample) only if (i) the IMF is more top heavy than assumed, or (ii) the dust extinction has been underestimated.

To explore this issue further, we show in Figure 5, pixel by pixel correlations of $\Sigma_{\text{SFR}}^{\text{H}\alpha}/\Sigma_{\text{SFR}}^{\text{FUV}}$ (both at 150 pc resolution) with Σ_{SFR} and Σ_{HI} (at 400 pc resolution). In each panel the hollow squares are for those galaxies for which the global $\Sigma_{\text{SFR}}^{\text{H}\alpha}$ is greater than the global $\Sigma_{\text{SFR}}^{\text{FUV}}$, while the filled circles are for those galaxies for which the global $\Sigma_{\text{SFR}}^{\text{H}\alpha}$ is less than the global $\Sigma_{\text{SFR}}^{\text{FUV}}$. From the first panel, one can clearly see that the anti correlation between $\Sigma_{\text{SFR}}^{\text{FUV}}/\Sigma_{\text{SFR}}^{\text{H}\alpha}$ and $\Sigma_{\text{SFR}}^{\text{H}\alpha}$ seen on global scales continues even on scales as small as 150pc. The right axis of the panels is the amount of differential dust obscuration required to bring the two SFR estimators into agreement. From Figure 5 one can see that bringing the two SFR estimators into agreement at the lowest star formation rates requires the dust obscuration to be more at $\text{H}\alpha$ than at FUV, which is physically implausible. It is more likely that one of the several mechanisms discussed above for suppressing the $\text{H}\alpha$ flux at low star formation rates is operative. At high star formation rates, where $\Sigma_{\text{SFR}}^{\text{H}\alpha} > \Sigma_{\text{SFR}}^{\text{FUV}}$, the average $N_{\text{HI}}/A_{\text{V}}$ required to bring the two estimators into agreement is 8, i.e. the gas should be about twice as dust rich as the SMC (for which $N_{\text{HI}}/A_{\text{V}}$ is 16.3 from Bouchet et al. (1985)). If one assumes that these regions have substantial molecular gas, and that the galaxies follow the L-Z relation for dwarfs (e.g. Ekta & Chengalur (2010)), and that dust is proportional to metallicity, then the required molecular gas densities to bring the gas to dust ratio to the same value as the SMC is $\Sigma_{\text{H}_2} \gtrsim 10^2 M_{\odot}/\text{pc}^{-2}$, similar to the peak densities in the center of spirals, which again seems unlikely. In summary it does not appear that dust extinction is the primary cause of the disagreement between $\Sigma_{\text{SFR}}^{\text{H}\alpha}$ and $\Sigma_{\text{SFR}}^{\text{FUV}}$ at the high Σ_{SFR} end.

In terms of direct observables, panel [B] shows that for the same amount of FUV emission, galaxies with lower global $\Sigma_{\text{SFR}}^{\text{H}\alpha}/\Sigma_{\text{SFR}}^{\text{FUV}}$ are under producing $\text{H}\alpha$ emission. This could either be because the galaxies have a fading starburst or because the galaxies are not producing high mass stars. Lee et al. (2009,a) find

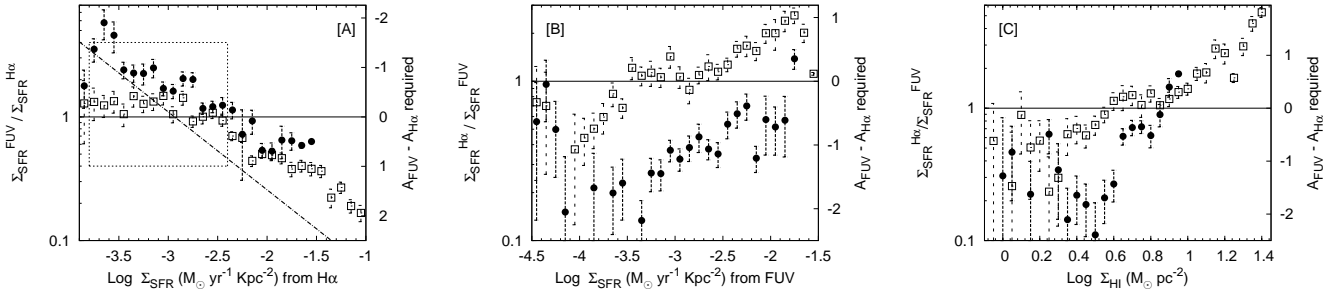


Figure 5. The ratio of $\Sigma_{\text{SFR}}^{H\alpha}$ and $\Sigma_{\text{SFR}}^{FUV}$ (at scales of 150 pc) plotted as a function of $\Sigma_{\text{SFR}}^{H\alpha}$ (Panel[A]), $\Sigma_{\text{SFR}}^{FUV}$ (Panel[B]) and Σ_{HI} (Panel[C]). The Σ_{HI} is computed from 400pc resolution images. The solid dots are for galaxies for which the global $\Sigma_{\text{SFR}}^{FUV} > \Sigma_{\text{SFR}}^{H\alpha}$, and the hollow square are for the galaxies with global $\Sigma_{\text{SFR}}^{H\alpha} > \Sigma_{\text{SFR}}^{FUV}$. Means and the errors on the mean for each bin are shown. The axes on the right show the amount of differential dust extinction required to bring the two SFR estimators into agreement. When binning in $\Sigma_{\text{SFR}}^{H\alpha}$ all pixels with $\Sigma_{\text{SFR}}^{H\alpha}$ more than 3 times the rms value (of the corresponding galaxy) are considered (regardless of the value of $\Sigma_{\text{SFR}}^{FUV}$), similarly, when binning in $\Sigma_{\text{SFR}}^{FUV}$ (and binning in Σ_{HI}) all pixels with $\Sigma_{\text{SFR}}^{FUV}$ more than 3 times the rms value are considered (regardless of the value of $\Sigma_{\text{SFR}}^{H\alpha}$). In Panel[A] the dotted rectangular region marks the area covered in the similar global plot Figure 2[C]. The dashed line in it is the best fit straight line from the global plot Figure 2[C].

that the frequency and amplitude of star bursts in dwarfs make the former explanation unlikely. However, a more detailed calculation, and observations of a larger sample would be needed to properly settle this issue. The most striking feature of the plots however is in panel [C], which shows that galaxies with lower global $\Sigma_{\text{SFR}}^{H\alpha}/\Sigma_{\text{SFR}}^{FUV}$ do not have gas with column density $\gtrsim 10M_{\odot}/\text{yr}$. The most straight forward interpretation of this is that massive star formation is more likely to happen in gas with high column densities. Indeed, star formation models have supported such a correlation (e.g. Krumholz et al. (2010)). While the linear scales that the models refer to are much smaller than those that we are dealing with here, such a correlation is likely given that high density star forming regions are more likely to occur in regions where the overall gas density is higher.

4 CONCLUSIONS

We find a clear stochasticity between the Σ_{HI} and Σ_{SFR} . All gas with $\Sigma_{\text{HI}} \gtrsim 10M_{\odot} \text{ pc}^{-2}$ has associated star formation. While the fraction of star forming gas decreases with decreasing Σ_{HI} there is no sharp “threshold” below which star formation is completely quenched. We also find that galaxies for which globally $\Sigma_{\text{SFR}}^{FUV} < \Sigma_{\text{SFR}}^{H\alpha}$ are marked by not having high HI column density (i.e. $\Sigma_{\text{HI}} > 10M_{\odot} \text{ pc}^{-2}$) gas. This is consistent with models in which formation of high mass stars preferentially happens in regions with high gas column density.

REFERENCES

Bigiel F., Leroy A., Walter F., Blitz L., Brinks E., de Blok W. J. G., Madore B., 2010, *AJ*, 140, 1194
 Begum A., Chengalur J. N., Hopp U., 2003, *NewA*, 8, 267
 Begum A., Chengalur J. N., Karachentsev I. D., Kaisin S. S., Sharina M. E., 2006, *MNRAS*, 365, 1220
 Begum A., Chengalur J. N., Karachentsev I. D., Sharina M. E., Kaisin S. S., 2008, *MNRAS*, 386, 1667
 Begum A., Chengalur J. N., Karachentsev I. D., Sharina M. E., 2008, *MNRAS*, 386, 138
 Bouchet P., Lequeux J., Maurice E., Prevot L., & Prevot-Burnichon M. L., 1985, *A&A*, 149, 330

Cardelli Jason A., Clayton Geoffrey C., & Mathis John S., 1989, *ApJ*, 345, 245
 Governato F., et al., 2010, *Nature*, 463, 203
 Ekta B., Chengalur J. N., 2010, *MNRAS*, 406, 1238
 Hunter Deidre A., Elmegreen Bruce G., & Ludka Bonnie C., 2010, *AJ*, 139, 447
 Kaisin S. S., & Karachentsev I. D., 2008, *A&A*, 479, 603
 Karachentsev I. D., & Kaisin S. S., 2007, *AJ*, 133, 1883
 Karachentsev I. D., Karachentseva V. E., Hutchmeier W. K., & Makarov D. I., 2004, *AJ*, 127, 2031
 Kennicutt Jr. Robert C., 1989, *ApJ*, 344, 685
 Kennicutt Jr. Robert C., 1998, *ApJ*, 498, 541
 Kennicutt Jr. Robert C., 1998a, *ARA&A*, 36, 189
 Krumholz M. R., Cunningham A. J., Klein R. I. & McKee C. F. 2010, *ApJ*, 713, 1120
 Lee Janice C. et al., 2009, *ApJ*, 706, 599
 Lee Janice C., Kennicutt Jr. Robert C., Funes S.J. Jose G., Sakai Shoko, & Akiyama Sanae, 2009a, *ApJ*, 692, 1305
 Leroy A. K., Walter F., Brinks E., Bigiel F., de Blok W. J. G., Madore B., Thornley M. D., 2008, *AJ*, 136, 2782
 Mac Low M.-M., Ferrara A., 1999, *ApJ*, 513, 142
 Melena N. W., Elmegreen B. G., Hunter D. A., Zernow L., 2009, *AJ*, 138, 1203
 Meurer Gerhardt R. et al., 2009, *ApJ*, 695, 765
 Pflamm-Altenburg Jan, Weidner Carsten, & Kroupa Pavel, 2007, *ApJ*, 671, 1550
 Pflamm-Altenburg J., Weidner C., & Pavel K. 2009, *MNRAS*, 395, 394
 Roychowdhury S., Chengalur J. N., Begum A., & Karachentsev I. D. 2009 *MNRAS*, 397, 1435
 Roychowdhury S., Chengalur J. N., Begum A., & Karachentsev I. D. 2010 *MNRAS*, 404, L60
 Schlegel David J., Finkbeiner Douglas P., & Davis Marc, 1998, *ApJ*, 500, 525
 Schmidt M., 1959, *ApJ*, 129, 243
 Skillman E.D., 1987, in Lonsdale Persson C. J., ed., *Star Formation in Galaxies*, NASA, p. 263
 Springel Volker et al., 2005, *Nat*, 435, 629
 Taylor C. L., Kobulnicky H. A., & Skillman E. D., 1998, *AJ*, 116, 2746
 Wong T., Blitz L., 2002, *ApJ*, 569, 157
 Weidner C., & Kroupa P., 2005, *ApJ*, 625, 754

This paper has been typeset from a $\text{T}_{\text{E}}\text{X}/\text{L}_{\text{A}}\text{T}_{\text{E}}\text{X}$ file prepared by the author.